

# A high-energy x-ray spectrometer diagnostic for the OMEGA laser

L. T. Hudson,<sup>a)</sup> A. Henins, and R. D. Deslattes<sup>b)</sup>

*National Institute of Standards and Technology, Gaithersburg, Maryland 20899*

J. F. Seely, G. E. Holland,<sup>c)</sup> R. Atkin,<sup>d)</sup> and L. Marlin

*Space Science Division, Naval Research Laboratory, Washington DC 20375*

D. D. Meyerhofer and C. Stoeckl

*Laboratory for Laser Energetics, University of Rochester, Rochester, New York 14623*

(Received 23 October 2001; accepted for publication 17 March 2002)

A new x-ray diagnostic has been commissioned at the OMEGA laser facility at the University of Rochester. It is a transmission curved crystal spectrometer designed primarily to characterize the hot-electron energy distribution of laser generated plasmas by registering the continuum x-ray spectrum produced by these hot plasmas from 12 to 60 keV. The diagnostic package is assembled in a linear configuration to ride in a standard instrument insertion module. The instrument consists of a nosecone with a blast shield, spectrometer, electronic imager, drive electronics, and battery. The instrument is connected to the external diagnostic processor and control unit by trigger and data fiber optic cables. Time integrated spectra from various targets have been registered with high sensitivity from single shots of the OMEGA laser. © 2002 American Institute of Physics.

[DOI: 10.1063/1.1476715]

## I. INTRODUCTION

Direct and indirect drive laser fusion target performance is limited by fast electron generation that can preheat the core plasma and adversely affect the compression and yield.<sup>1</sup> It is important to characterize the hot-electron energy distribution of plasmas produced under research conditions. The purpose of the present instrument is to address this issue by registering the hard x-ray Bremsstrahlung spectrum emitted by the plasma. Such studies of the continuum x-ray distribution are relevant to implosion experiments on the OMEGA laser facility<sup>2</sup> at the Laboratory for Laser Energetics (LLE) and preparations for experiments on the National Ignition Facility. To this end, we report the progress of a newly commissioned high-energy x-ray spectrometer (HXS) at the OMEGA laser facility which has been designed to cover the 12–60 keV spectral range. In addition to its primary mission, it can be applied to >10 keV x-ray backlighter development, x-ray conversion studies, and basic atomic physics experiments.

## II. OPTICAL DESIGN

The optical design of the spectrometer is shown in Fig. 1<sup>3</sup> and is an adaptation of a compact and robust instrument originally developed at the National Institute of Standards and Technology (NIST) for the energy calibration of medical radiography x-ray sources.<sup>4–6</sup> The design is a combination of the curved crystal optics proposed by Cauchois<sup>7</sup> with the

symmetric transmission geometry due to Rutherford and Andrade.<sup>8</sup> The spectrometer is composed of a cylindrically bent crystal, a slit, a scatter shield, and a charge coupled device (CCD) detector with 1360 rows and 1840 columns of pixels. The sensor is a relatively low-cost dental CCD from TREX Medical Corporation<sup>9</sup> and the associated electronics digitizes each pixel at 8 bit resolution. The sensor is enclosed in a light-tight housing with an entrance window of black plastic. The instrument produces two mirror-symmetric spectra on the detector plane using a symmetric transmission (Laue case) diffraction geometry; the view in Fig. 1 is the plane of diffraction. In this geometry, dispersed x rays pass through a polychromatic crossover point and are focused onto the Rowland circle, whose diameter equals the radius of curvature of the crystal. The planar detector is positioned perpendicular to the center line connecting the source and detector and such that it intersects the Rowland circle at two points which correspond to an energy in the midrange of a typical spectrum. The zero wavelength position of each of the two mirror-symmetric spectra falls on this center line; increasing wavelengths are registered in the detector plane at increasing distances from the center line. The quartz crystal has been aligned, cut, and mounted so that the (10 $\bar{1}$ 1) diffracting planes (3.34 Å lattice spacing) are perpendicular to the crystal surface. After polishing the quartz crystal to a thickness of about 220  $\mu\text{m}$ , it was etched in ammonium bifluoride to remove surface damage, and then bent elastically to a cylindrical radius of 112 mm. During instrument validation, the crystal is rotated until the midpoint between the two mirror-symmetric spectra coincides with the pinhole image of an x-ray source situated on the center axis of the instrument. Finally, the sensor is rotated around this center axis to

<sup>a)</sup>Author to whom correspondence should be addressed; electronic mail: larry.hudson@nist.gov

<sup>b)</sup>Deceased.

<sup>c)</sup>Present address: SFA, 9315 Largo Dr., West Suite 200, Largo, MD 20774.

<sup>d)</sup>Present address: Tiger Innovations, L.L.C., 3610 North Vacation Lane, Arlington, VA 22207.

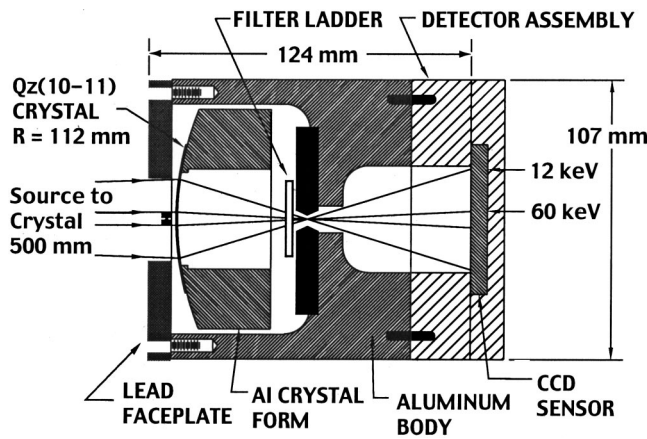


FIG. 1. Optical layout of the HXS curved crystal spectrometer.

make the spectral lines appear vertical in the CCD image, thereby bringing the pixel columns coincident with the diffracting planes.

Having aligned the spectrometer and acquired an x-ray image, a column sum of the pixel values gives a one-dimensional “lineout” spectrum. The instrumental zero wavelength position coincides with the bisector of any pair of corresponding spectral features. This permits the energy axis to be self-calibrated using a few x-ray lines or absorption edges of known energy. Although the wavelength dispersion is approximately constant, a very good approximation of the “plate function” which relates lateral position on the detector to x-ray energy is given by<sup>5</sup>

$$E^2 = a + b/x^2,$$

where  $a$  and  $b$  are constants,  $x$  is the lateral distance from the spectrometer center line to any spectral feature of interest, and  $E$  is the energy registered at  $x$ .

The HXS spectrometer geometry has been designed such that at a 0.5 m source-to-crystal standoff distance, 12 keV x rays are registered at the outermost column of the CCD (18 mm from center line) while that collected at 60 keV strike the detector about 3.5 mm from center. To verify the plate function, we have used the  $K$ -absorption edges of Sn, Cd, Mo, and Zr filters as well known energy markers.<sup>10</sup> These foils of 25–50  $\mu\text{m}$  thickness were inserted into the spectrometer just before the polychromatic focal point via a filter assembly which is inserted through the lid of the spectrometer body. Examples of spectra with and without the introduction of edge structure are given in Fig. 2 after normalization against fixed-pattern noise of the CCD response. These data were acquired with a molybdenum laboratory microfocus x-ray source (0.2 mm focal spot) positioned 0.5 m from the crystal and operated at 42 kV and 0.7 mA. The edge position is taken to be the inflection point in the absorption curve, which is proportional to the logarithm of the acquired filtered spectrum.<sup>11</sup> The experimentally realized plate function is shown in Fig. 3(a) as a fit through the four experimental calibration points indicated with solid dots. In this calibration exercise with input data coordinates having units of pixels and eV, the fitting constants were  $a = 6.420e6$ ;  $b$

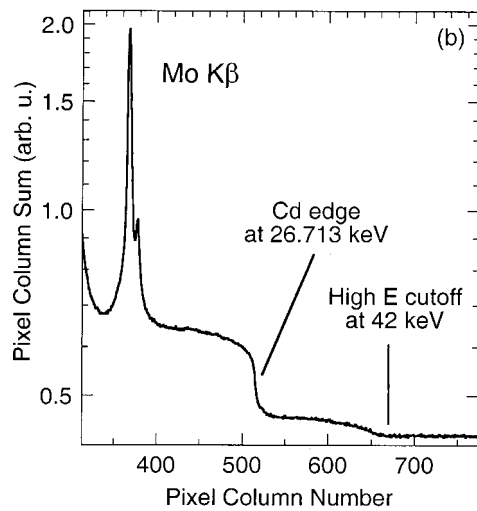
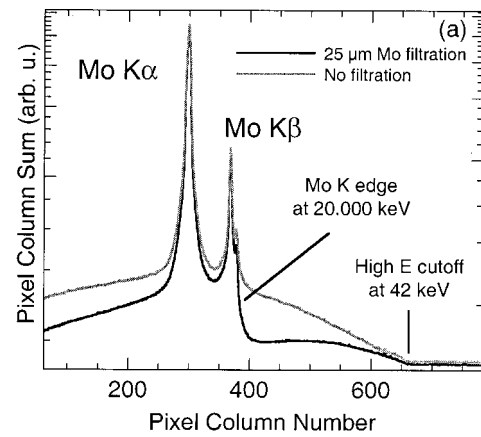


FIG. 2. Spectra acquired with a molybdenum laboratory x-ray source positioned 0.5 m from the crystal. The x-ray tube was operated at 42 kV and 0.7 mA. (a) Spectra registered with and without 25  $\mu\text{m}$  of Mo filtration upon 53 mA s of exposure. For comparison of shapes, the two spectra are scaled. (b) Spectrum obtained with 50  $\mu\text{m}$  of Cd filtration with 31 mA s of exposure.

$= 1.110e14$ . The residuals between data and fit had a 1  $\sigma$  standard deviation of 0.05 keV.

While the crystal resolving power is several thousand and the CCD pixel size is only 19.5  $\mu\text{m}$ , the instrumental resolution is about 4 pixels at Mo  $K\alpha$  (17.4 keV) and is dominated by scattering in the  $\text{Gd}_2\text{O}_2\text{S:Tb}$  x-ray phosphor converter of finite thickness that is presently in use (not vendor supplied). We have found this same spatial resolution using this screen with a pixilated sensor with twice the pixel dimensions as the present CCD. This resolution element was determined by modeling the measured Mo  $K\alpha$  doublet with Lorentzian natural linewidths (of about 6.4 eV)<sup>12</sup> convolved with a Gaussian instrumental line spread function. The full width at half maximum of the instrumental line spread function thus found to best model the data is multiplied by the slope of the instrumental dispersion [Fig. 3(a)] to predict the resolving power as a function of x-ray energy as shown in Fig. 3(b). The resolving power so computed ranges from about 250 at the lowest energies to about 50 at 60 keV. This analysis neglects any energy dependence of the detector line spread function. Since continuum studies were the primary focus for HXS, high resolving power was not a primary design driver; however, if higher resolution were needed in the

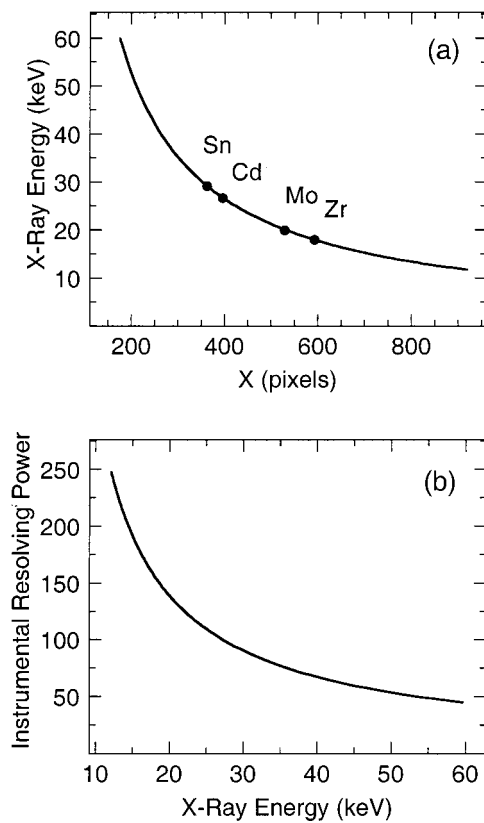


FIG. 3. (a) Empirically determined plate function for the crystal spectrometer at 0.5 m source-to-crystal standoff distance.  $X$  is the distance in the dispersion direction in pixels from any spectral feature of energy  $E$  to the spectrometer center axis. The four calibration points are the positions found for the  $K$  absorption edges of the four elemental foils indicated and the curve is a fit using the form of dispersion equation. (b) Instrumental resolving power determined as a product of the slope of the plate function (a) and a resolution element of 4 pixels ( $78 \mu\text{m}$ ).

future, this could readily be achieved by employing a thinner phosphor conversion layer in front of the CCD or x-ray sensitive film in place of the CCD for very fine spectral resolution.

One of the advantages of using a Rowland-circle geometry is the relative insensitivity of measured spectral linewidths to source size. Monte Carlo ray-tracing software has been applied to the geometry of the HXS spectrometer with 0.5 m source-to-crystal distance to predict its sensitivity to source size.<sup>13</sup> Only lateral source width in the plane of diffraction would affect the spectral resolution. Calculations were performed for source widths up to 13 mm at 39 keV with the result that these could contribute up to  $15 \mu\text{m}$  to line broadening. Since this is much less than the effective instrumental resolution, modest source size is not expected to cause significant degradation of the instrumental resolution. Experimental tests were also performed to determine the roll, pitch, and yaw pointing precision requirements and field of view of HXS using a laboratory x-ray source at a distance of 0.5 m from the crystal. Roll angle alignment (about the center axis of the instrument) should not influence the results acquired from a symmetric source. Instrument or source pitch-angle misalignment causes the entire spectrum to shift up or down on the sensor (perpendicular to the dispersion plane) and would not significantly affect energy determina-

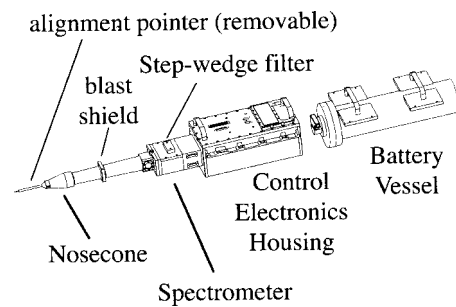


FIG. 4. Mechanical layout of the HXS diagnostic.

tion but could result in some loss of signal. Yaw errors, if small, are well compensated by averaging distances from the fiducial detector center to corresponding features in each of the two mirror spectra. Gross yaw errors can violate the diffraction condition or cause other vignetting, resulting in the partial or complete loss of one or both of the mirror-symmetric spectra. Tests showed that the instrument has a lateral field of view of about  $\pm 0.35^\circ$ , which represents about  $\pm 3 \text{ mm}$  at the target. We note that in practice both relative pitch and yaw pointing errors can be readily quantified by noting the position of the x-ray pinhole image on the CCD relative to its fiducial position.

### III. MECHANICAL DESIGN

The HXS diagnostic was mechanically designed to be modular and to stay within the operating envelope of an LLE ten-inch instrument manipulator (TIM). The modularity of the diagnostic allows system components to be removed, serviced, or replaced with as little “down time” as possible. Alignment between principal diagnostic components is maintained with the use of 3 mm diam dowel pins. Lead shielding and apertures are used throughout to reduce sensor fogging by high-energy particles and x rays. All fasteners used in the system are captive so that maintenance, such as changing a filter, can be performed in cleanroom attire without the concern of lost hardware within the TIM. Finally, to provide an inexpensive and user-friendly diagnostic, the system was designed with off-the-shelf hardware, common materials, and proven technology.

The procedure to establish the HXS standoff distance and alignment begins with bolting the diagnostic into the TIM. Centering is established by tooling balls on the diagnostic and receptacles on the TIM support rails. A pointer assembly is then kinematically attached to the diagnostic nosecone. On the tip of the pointer is an  $800 \mu\text{m}$  diam sphere whose position is referenced to the tooling ball receptacles. The pointer assembly is shown in the high-level overview of the principal HXS components in Fig. 4. After evacuating the TIM, it is inserted into the 3 m diam OMEGA target chamber which is held at a vacuum of  $\approx 10^{-6}$  Torr. The diagnostic is then aligned and positioned to target chamber center using two orthogonal-viewing cameras trained on the tip of the pointer. After alignment, the instrument module is retracted and the pointer removed. The diagnostic can then be redeployed with a reproducible pointing precision of about 0.05 mm.

A 0.14 mm thick Be foil is used as a blast shield. It is located in the nosecone assembly in front of the spectrometer as shown in Fig. 4 and is easily extracted and replaced. Sintered plugs are held in the flanges shown near the spectrometer end of the nosecone to facilitate evacuation of the diagnostic before insertion into the target chamber; such plugs are also placed at other locations along the diagnostic. The location of the step-wedge filter is also shown in Fig. 4; it can be interchanged from the top of the spectrometer body. Behind the spectrometer are the drive electronics which will be described in detail in Sec. IV. Finally, in the rear of the diagnostic, internal power is provided by a standard vacuum vessel containing 42-nickel cadmium “D” size rechargeable battery cells. This provides all the power needed by the diagnostic and the only connections to outside the TIM are two fiber optic cables and cooling water for the electronics. This permits the diagnostic to be surrounded by a Faraday cage to reduce its susceptibility to facility-induced electromagnetic interference. The battery is removed from the TIM and recharged offline. The battery has operated in the diagnostic under full load for up to 16 h.

#### IV. ELECTRONIC DATA ACQUISITION AND CONTROL SYSTEM

The electronic data acquisition and control system for HXS consists of a diagnostic control processor (DCP), a diagnostic interface unit (DIU) and drive electronics (DE). The conceptual relationship of these three systems is shown in Fig. 5. Together they control the instrument, while allowing the instrument to remain in a Faraday cage inside the TIM. This capability is made possible by operating the instrument from battery power only, and communicating between the instrument and the control electronics external to the TIM via two fiber-optic links (trigger and data transceiver).

The DCP is the master intelligent control for the system, and the primary interface between the HXS diagnostic and the facility data acquisition system (FDAS). The DCP software controller receives messages from the FDAS and performs the necessary control functions. It commands the instrument to different power states, forwards any control parameters, configures and arms the instrument for the trigger pulse indicating a shot, downloads the image data, and stores the data on the FDAS network file system. During these processes, the controller is collecting telemetry from the instrument and the DIU, including temperatures and operating voltages. The DCP is located outside the target bay and may be operated remotely over the local area network.

The DIU is an electrical/optical interface and the only connection between the FDAS and the instrument. The DIU contains a custom fiber-optic modem that allows full duplex serial communication via a single fiber. The second fiber is used to propagate the timing pulse. The DIU provides a visual indication of the trigger status and quality of the fiber optic link (synchronized connection and error status). The DCP can instruct the DIU to arm for trigger (that is to propagate any received electrical timing pulse over the fiber optic link), or generate a trigger (simulate receipt of a timing pulse). There is a fiber-optic patch panel at the DIU site

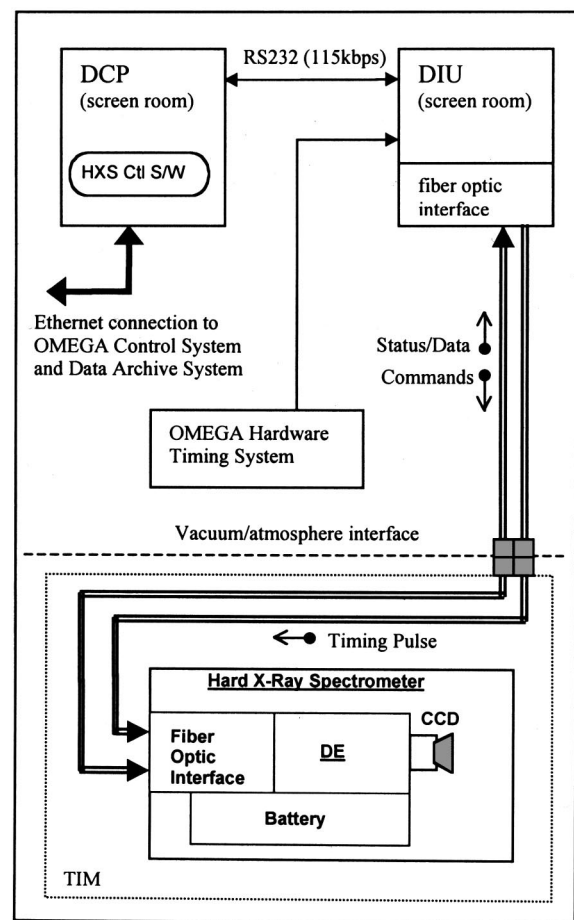


FIG. 5. Schematic of the electronic data acquisition and control system.

enabling the DIU to be connected to any TIM position.

The final part of the electrical control system is the DE (located in the TIM) which consists of a control processor and a CCD interface. The CCD interface contains a slave PC104 computer and the fiber-optic interface board. The control processor includes several custom electronics boards to control the timing and power of the instrument, as well as to monitor temperatures and voltages inside the instrument. The control processor interfaces with a fiber optic transceiver modem to enable serial communication with the support equipment. It also interfaces to a fiber-optic receiver to convert the incoming optical trigger pulse. This trigger pulse is used as the starting point of a data collection cycle. Upon receipt of the trigger, the CCD is cleared after a software-commanded delay (with submillisecond precision). After another software controlled delay of submillisecond precision, the CCD integration is initiated for a duration of submilliseconds to several hours. In general, the CCD is integrated for about 1 s spanning the laser shot. These control points (along with a serial communication link) are used to determine the operation of the CCD interface. The CCD interface consists of a Trex Trophy<sup>9</sup> CCD driver board and a PC104 computer. The CCD driver board receives the clear and integrated signals for collection of images from the CCD. After the commanded integration time is complete, the CCD driver board clocks the data out of the CCD with 12-bit sampling precision. A limitation of the current commercial CCD driver is

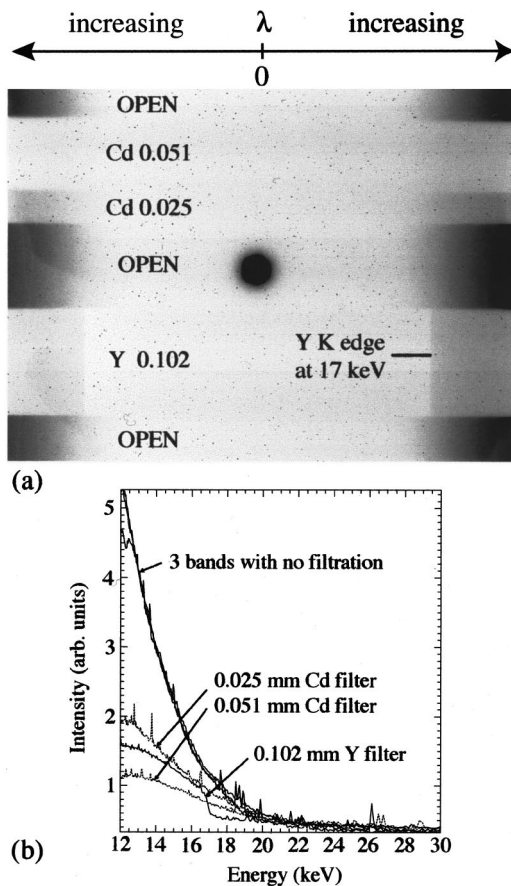


FIG. 6. (a) First spectrum acquired by HXS. The target was 3 bar of deuterium in a thin plastic shell. The value shown associated with each filter of Cd and Y is the foil thickness in mm. (b) Lineout spectra from differently filtered regions of the image placed on an energy scale using the dispersion relation of Fig. 3(a).

that it autoscales and truncates the data to 8-bit precision, precluding absolute intensity calibration of the diagnostic. Efforts are underway to upgrade to a custom-built CCD driver board that will return the raw 12-bit precision sampled data allowing any desired postprocessing with custom software.

## V. FIRST EXPERIMENTAL RESULTS

The HXS diagnostic was designed primarily to study continuum x-ray emission from the laser produced plasmas at OMEGA. The first spectrum registered was from the implosion of deuterium gas held at 3 bar in a polymer shell 24  $\mu\text{m}$  thick. The TIM was inserted such that the crystal was 0.5 m from the center of the 1.524 m radius target chamber. The  $\text{D}_2\text{-CH}$  target was spherically irradiated by 60 laser beams with a total of 23 kJ in a 1 ns square pulse. Filtration included a 0.14 mm Be blast shield in the nosecone and a filter assembly inserted at the polychromatic focal point of the instrument; these filters were Cd and Y with thickness steps perpendicular to the dispersion direction. The foil thicknesses are indicated on the CCD image of Fig. 6(a) in millimeters. The column sums of digitized pixel values from the six horizontal bands shown in the CCD image were normalized to the number of rows summed in each band. Then using the calibration plate function discussed in Sec. II, these

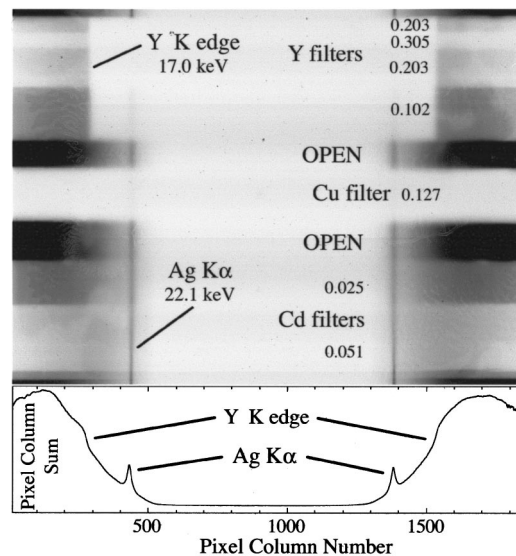


FIG. 7. Image and spectrum (pixel column sum of the entire image) produced by 24-beam irradiation of a Ag foil. The unlabeled numbers on the figure represent the thickness of the indicated foils in mm.

sums are plotted against energy in Fig. 6(b) to obtain spectral information. The 1 pixel wide spikes are from saturated pixels surrounded by areas of unsaturated pixels; their position is not reproducible and these are presumably due to direct CCD detection of undispersed highly energetic particles or x rays. The yttrium *K* absorption edge at 17.04 keV is clearly seen in both the image and the *Y*-filter lineout spectrum, but the x-ray flux distribution was not sufficiently energetic to permit observation of the cadmium *K* edge at 26.7 keV. The pinhole image shows gross pixel blooming owing to lack of filtration. Even so it was possible to determine a 7 pixel lateral relative misalignment of source and instrument compared to the fiducial pixel coordinates determined at NIST during instrument validation. This corresponds to 0.6 mm at the target standoff distance and accounts for the uneven exposure visible between the left and right sides of Fig. 6(a).

In another experimental run and with superior alignment to the target, the large face of a 2 mm  $\times$  2 mm  $\times$  25  $\mu\text{m}$  Ag foil was positioned to face the HXS diagnostic and was irradiated by 24 beams on both sides. The CCD output registered during the 1 ns exposure is shown in Fig. 7 along with a pixel column sum of the entire image which considerably enhances the dynamic range per bandwidth compared to the 8-bit depth of each pixel. The CCD was integrated for a total of 1 s at room temperature; no dark image has been subtracted. While the image contrast has been adjusted for presentation, only 1 pixel in 10 000 was saturated in these data. Energy is increased toward the center of the image and the vertical banding is due to filters of Y, Cu, and Cd; the thickness of each filter is indicated in the figure in mm. No pinhole image is observed in the center of this image because of the 0.127 mm of Cu filtration across the center of the image and an additional 1 mm of Ti filtration over the pinhole itself. On shots with less filtration, the pinhole image was observed and was about 0.7 mm in diameter. The pinhole filter support could also be adjusted to an open or closed setting.

This image illustrates not only registration of the con-

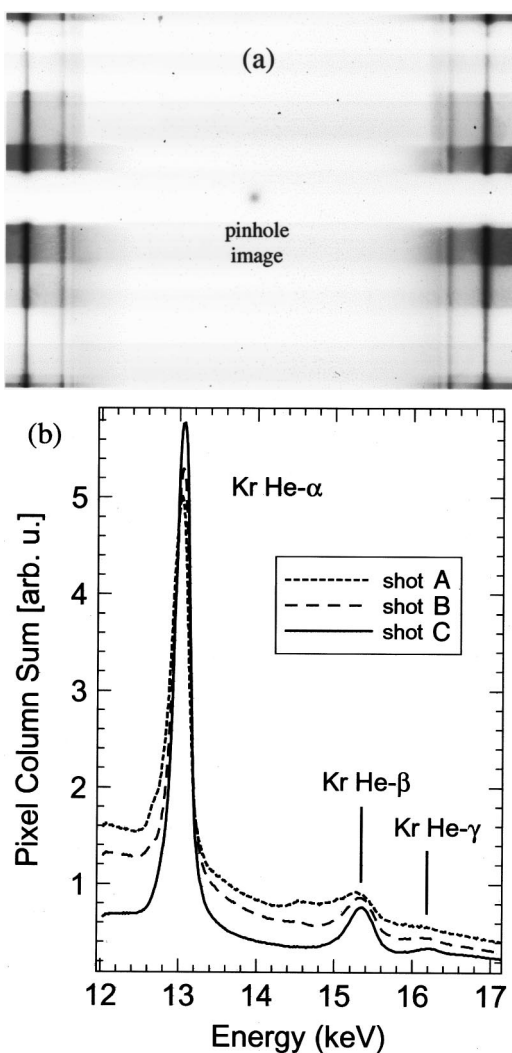


FIG. 8. (a) HXS image from a CH shell target containing  $H_2$ ,  $D_2$ , and Kr. The filtration is the same as Fig. 7. (b) Helium-like krypton resonance line series spectrum from three OMEGA shots.

tinuum spectrum produced by this target with 24 kJ of beam energy, but also *in situ* spectral markers such as the yttrium filter  $K$  absorption edge at 17 keV and the Ag  $K\alpha$  emissions at 22 keV from the foil itself. The cadmium edge is not discernible as it falls very near the high energy limit of this Bremsstrahlung spectrum. Such internal markers are useful for *in situ* checks of the energy calibration should the source of x rays be positioned transversely off the instrument center axis. The images in Figs. 6 and 7 also exhibit some small scale structure which is artificially introduced due to the imperfect mating of the x-ray converter screen to the face of the CCD using optical grease. This situation has greatly improved with vacuum cycling as air pockets have been removed.

As a final example of the diagnostic utility of HXS, the resonance lines from helium-like  $Kr^{+34}$  are shown in Fig. 8.

The target consisted of a plastic shell filled with 8 bar of hydrogen, 2 bar of deuterium, and a 1% trace of krypton. The shell had an outer diameter of 894  $\mu\text{m}$  and a wall thickness of 10.8  $\mu\text{m}$ . This target was spherically irradiated by 60 beams (21.8 kJ total laser energy). The resultant image [Fig. 8(a)] used the same filter pack as indicated in Fig. 7 and the pinhole filter was in the open position. The darkest bands above and below the pinhole image (open areas in the filter pack) were column summed and the left side of the resultant spectrum is shown in Fig. 8(b) for three successive laser shots. Shot A had a laser energy of 21.8 kJ; shot B, 26.7 kJ; and shot C, 17.4 kJ. The wavelengths of the Kr lines labeled in Fig. 8(b) have been calculated to fall at 13.11, 15.43, and 16.25 keV;<sup>14</sup> He  $\alpha$  denotes the transition  $1s2p\ ^1P_1 - 1s^2\ ^1S_0$ ; He  $\beta$ ,  $1s3p$ , etc. Our energy scale finds the peaks about 0.05 keV below the tabulated values of Ref. 11. 0.05 keV is also the magnitude of the standard uncertainty of the HXS energy calibration curve. The systematic discrepancy, however, may be due largely to the presence of lithium-like and beryllium-like dielectronic satellites, seen in varying degrees of prominence, on the low-energy side of the resonance lines. It has been shown<sup>15</sup> that the intensity ratios of lines such as these may be used along with hydrodynamic simulations to determine the electron temperature of the plasma.

#### ACKNOWLEDGMENTS

This work was supported, in part, by the U.S. Department of Energy Office of Inertial Confinement Fusion under Cooperative Agreement No. DE-FC03-92SF19460, the University of Rochester, and the New York State Energy Research and Development Authority. The support of DOE does not constitute an endorsement by DOE of the views expressed in this article.

<sup>1</sup>W. L. Kruer, *The Physics of Laser-Plasma Interactions* (Addison-Wesley, Redwood City, CA 1988).

<sup>2</sup>T. R. Boehly *et al.*, Rev. Sci. Instrum. **66**, 508 (1995).

<sup>3</sup>U.S. Patent No. 5,381,458 (1995).

<sup>4</sup>R. D. Deslattes, J. C. Levin, M. D. Walker, and A. Henins, Med. Phys. **21**, 123 (1994).

<sup>5</sup>L. T. Hudson, R. D. Deslattes, A. Henins, C. T. Chandler, E. G. Kessler, and J. E. Schweppe, Med. Phys. **23**, 1659 (1996).

<sup>6</sup>C. T. Chantler, R. D. Deslattes, A. Henins, and L. T. Hudson, Br. J. Radiol. **69**, 636 (1996).

<sup>7</sup>Y. Cauchois, J. Phys. Radium **3**, 320 (1932); outlined in A. H. Compton and S. K. Allison, *X-Rays in Theory and Experiment* (Van Nostrand, New York, 1935), p. 750.

<sup>8</sup>E. Rutherford and E. N. da C. Andrade, Philos. Mag. **28**, 263 (1914).

<sup>9</sup>The equipment identified in this article is to specify the experimental procedure and does not imply endorsement or recommendation, nor is it intended to imply that it is the best available for the purpose.

<sup>10</sup>R. D. Deslattes, E. G. Kessler, Jr., P. Indelicato, and E. Lindroth, *International Tables for Crystallography*, Vol. C (Kluwer Academic, Dordrecht, The Netherlands, 1999), p. 200.

<sup>11</sup>S. Kraft, J. Stumpel, P. Becker, and U. Kuetsgens, Rev. Sci. Instrum. **67**, 681 (1996).

<sup>12</sup>M. O. Krause and J. H. Oliver, J. Phys. Chem. Ref. Data **8**, 329 (1979).

<sup>13</sup>H. F. Beyer, Nucl. Instrum. Methods Phys. Res. A **400**, 137 (1997).

<sup>14</sup>L. A. Vainshtein and U. I. Safronova, Phys. Scr. **31**, 519 (1985).

<sup>15</sup>B. Yaakobi, F. J. Marshall, and R. Epstein, Phys. Rev. E **54**, 5848 (1996).